IOP PUBLISHING CLASSICAL AND QUANTUM GRAVITY

Class. Quantum Grav. **24** (2007) 1457–1477 doi:10.1088/0264-9381/24/6/006

Response of resonant gravitational wave detectors to damped sinusoid signals

A Pai[1,4], C Celsi[1,2], G V Pallottino[1,2], S D'Antonio[3] and P Astone[1]

[1] INFN, Sezione Roma 1—P.le Aldo Moro, 2 00185 Roma, Italy
[2] Department of Physics, University of Roma La Sapienza, Roma, Italy
[3] INFN Sezione Roma 2 Tor Vergata, Roma, Italy

E-mail: Archana.Pai@aei.mpg.de and pallottino@roma1.infn.it

Received 16 October 2006, in final form 10 December 2006
Published 6 March 2007
Online at stacks.iop.org/CQG/24/1457

Abstract

Till date, the search for burst signals with resonant gravitational wave (GW) detectors has been done using the δ-function approximation for the signal, which was reasonable due to the very small bandwidth of these detectors. However, now with increased bandwidth (of the order of 10 or more Hz) and with the possibility of comparing results with interferometric GW detectors (broad-band), it is very important to exploit the resonant detectors' capability to detect also signals with specific wave shapes. As a first step, we present a study of the response of resonant GW detectors to damped sinusoids with given frequency and decay time and report on the development of a filter matched to these signals. This study is a preliminary step towards the comprehension of the detector response and of the filtering for signals such as the excitation of stellar quasi-normal modes.

PACS numbers: 04.80.Nn, 07.05.Kf, 95.55.Ym

(Some figures in this article are in colour only in the electronic version)

1. Introduction

A GW resonant detector consists of a large, solid heavy (a few tons) bar, made of low loss material (usually aluminium). The incoming GW can excite the first longitudinal mode of the bar. These mechanical oscillations produce displacement of the bar end face, where a low mass electrical transducer is attached with resonance frequency close to that of the bar. This transducer converts the mechanical vibration into an electrical signal which then is amplified by a low noise electronic chain. At present, the ROG gravitational wave (GW) resonant bars, Explorer and Nautilus, are operating at the sensitivity level of $h \sim 3 \times 10^{-21}\,\mathrm{Hz}^{-1/2}$. The

[4] Present address: Max Planck Institut für Gravitationsphysik (AEI), Am Mühlenberg 1, D-14476 Potsdam, Germany.

improvement in the read-out of these detectors has broadened the bandwidth (BW) [1] from a fraction of a Hz to $\sim$ 20 Hz at the level of $h \sim 10^{-20}\,\mathrm{Hz}^{-1/2}$. The resonant bar AURIGA, with a three-mode detection scheme, is operating at $h \sim 1.5 \times 10^{-21}\,\mathrm{Hz}^{-1/2}$ with a bandwidth of more than 100 Hz at $h \sim 10^{-20}\,\mathrm{Hz}^{-1/2}$ [2].

Broader BW opens up the possibility of looking for short burst signals with different shapes in resonant detectors in contrast to looking for 'simple' impulses as is done till date. The filtering techniques for detecting impulse-like signals are based on the assumption that the spectrum of these signals is approximately flat in the detector's narrow band [4]. The response of a resonant detector to such impulse-like GW was studied and understood in detail. However, with the new development mentioned above, it is worth studying how resonant bars will respond to GW of different shapes and how their increased BW will affect the detector response, in view of opening a new range of detectable signals.

A large number of astrophysical scenarios, such as merger of two neutron stars (NS) or black-holes (BH), core collapse of massive stars during the end stages of stellar evolution, accretion of matter, rotational instabilities in newly born rapidly rotating stars, can excite stellar quasi-normal modes (QNM). The resultant QNM ringing radiates energy in the form of damped sinusoid GW, with damping time and frequency depending on the underlying physical dissipation processes. In a recent review [5], various astrophysical scenarios are listed which might emit such GW.

One such plausible scenario is the QNM ringing during the end stage of stellar evolution. After the core collapse, when the proto-neutron star is going through the cooling phase, various QNM are excited. In particular, the fundamental mode emits GW in the frequency range of (850–1000) Hz with frequency as well as damping time evolving as a function of time [6] and thus can fall and may chirp in the BW of the current resonant bars.

In this paper, as a preliminary step, we study a simple case of an impinging GW radiated from stellar QNM, which we model here as a damped sinusoid with fixed frequency and damping time:

$$h(t) = h_0 \sin[\omega_0(t - t_0)]\, \mathrm{e}^{-(t-t_0)/\tau}\theta(t - t_0). \tag{1}$$

Here $\theta(t - t_0)$ implies $h(t) \neq 0$ for $t \geqslant t_0$, $f_0 = \omega_0/(2\pi)$ is the signal frequency and τ is the damping time. The root-sum-square (rss) amplitude spectral density [7] in units of strain per root Hz for the above signal is

$$h_{\mathrm{rss}} = h_0\sqrt{\tau}/2. \tag{2}$$

The study of more complex QNM evolution—damped sinusoid GW with varying frequency and damping time—is left for the future work. As for the damping time, astrophysical inputs [5] suggest that the GW signal from stellar QNM lasts from a fraction of a second to a few seconds. Thus, our study is restricted to a maximum value of τ of a second. This study is performed to understand how a detector's response is different from that to impulse-like signals, which will help in constructing the filters.

The paper is divided as follows. In section 2, we discuss the bar–transducer system transfer function. In section 3, we derive the system response to a damped sinusoid GW signal, identifying the terms of the response which are associated with the 'detector modes' and with the signal itself. The system response due to impinging GW gets amplitude as well as phase modulated. We study in section 4, the features of this modulation for different cases and for various values of the signal parameters. Finally, in section 5, we derive and discuss the matched filter transfer function and the expression for the SNR. In the conclusion, we address also some points for future work.

2. The system transfer function

The bar–transducer system of some resonant bar detectors can be modelled as a coupled harmonic oscillator system with two resonant modes $f_\pm$ [4]. Our analysis is based on this simple model, which represents fairly well the actual behaviour of detectors such as Explorer and Nautilus. Future extensions of this work may consider three-mode detectors, as AURIGA [2], or multi-mode detectors, as MINIGRAIL [3]. The incoming GW, denoted by $h(t)$, provides an equivalent external force

$$f_x(t) = m_x L\ddot{h}(t)/2 \tag{3}$$

to the bar, with corresponding displacements $x(t)$ for the bar and $y(t)$ for the transducer. Here, $m_x = M_{\rm bar}/2$ is the reduced mass of the bar and $L = 4L_{\rm bar}/\pi^2$ is its effective length. The electrical output of the transducer is proportional to the relative displacement of the transducer and the bar, $u(t) = y(t) - x(t)$ from their equilibrium positions. In Fourier domain[5] this displacement due to the external force $f_x(t)$ is obtained from

$$U(\mathrm{j}\omega) = W_{ux}(\mathrm{j}\omega)F_x(\mathrm{j}\omega), \tag{4}$$

where $F_x(\mathrm{j}\omega)$ is the Fourier transform (FT) of $f_x(t)$ and $W_{ux}(\mathrm{j}\omega)$ is the system transfer function from the input force $f_x(t)$ to the output displacement $u(t)$ obtained from the equations of motion of the forced coupled harmonic oscillator [4]:

$$W_{ux}(\mathrm{j}\omega) = \frac{\omega^2}{m_x \prod_{i=1}^{4}(\omega - \omega_i)}. \tag{5}$$

The system poles ω_i are

$$\omega_1 = -\omega_+ + \mathrm{j}/\tau'_+ \qquad \omega_2 = -\omega_1^*, \tag{6}$$

$$\omega_3 = -\omega_- + \mathrm{j}/\tau'_- \qquad \omega_4 = -\omega_3^*, \tag{7}$$

where $\omega_\pm = 2\pi f_\pm$. The $\tau'_\pm$ are the decay times of the two resonant modes and are related to the dissipation factors of the coupled oscillators $\beta_\pm$ by $\tau'_\pm = 1/\beta_\pm$ [4], with corresponding merit factors $Q_\pm = \beta_\pm/2\omega_\pm$. The mechanical oscillators of resonant detectors are designed with large Q-factors (usually in the range 10^5–10^7) in order to increase their sensitivity, which means $\beta_\pm \ll 1$. The displacement $u(t)$, measured in units of length, is obtained by the inverse FT of $U(\mathrm{j}\omega)$.

3. System response to a damped sinusoidal GW signal

In order to study the response of the system to a specific input GW $h(t)$—in our case a damped sine-wave—one requires to calculate the force and then obtain the displacement $u(t)$ from equations (4), (5). In this section, we derive the system response and study its features.

Using equation (3), we calculate the external force on the bar due to the incoming $h(t)$ given by equation (1):

$$f_x(t) = \frac{h_0 m_x L}{2}\left(\left[\left(\frac{1}{\tau^2} - \omega_0^2\right)\sin[\omega_0(t-t_0)] - \frac{2\omega_0}{\tau}\cos[\omega_0(t-t_0)]\right]\right.$$
$$\left.\times\, \mathrm{e}^{-(t-t_0)/\tau}\theta(t-t_0) + \omega_0\delta(t-t_0)\right). \tag{8}$$

[5] We follow the convention of representing with lower cases the signals in time domain and with capitals their Fourier transforms.

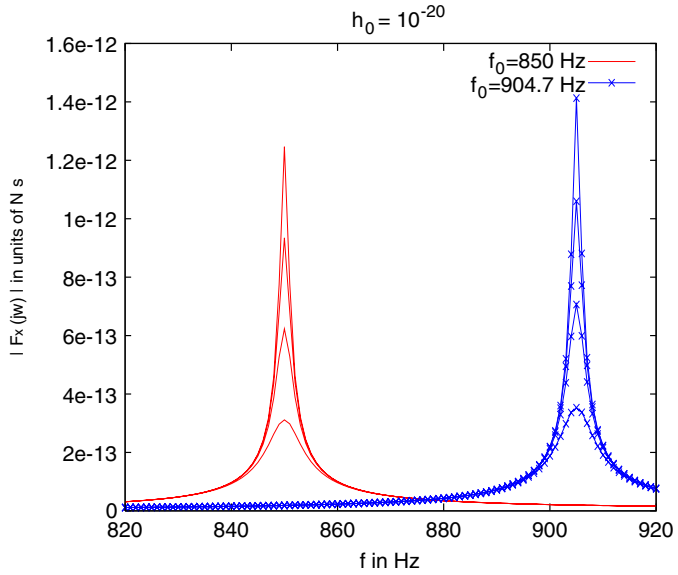

Figure 1. Spectra of $|F_x(\mathrm{j}\omega)|$ for $h_0 = 10^{-20}$, $f_0 = 850$ and 904.7 Hz, $\tau = 50, 100, 150, 200$ ms, with $M_{\mathrm{bar}} = 2230$ kg and $L_{\mathrm{bar}} = 3$ m (Explorer parameters). The higher the value of τ, the higher the peak of $|F_x(\mathrm{j}\omega)|$.

Its FT in terms of $H(\mathrm{j}\omega)$ is

$$F_x(\mathrm{j}\omega) = \frac{-m_x L\omega^2}{2} H(\mathrm{j}\omega), \tag{9}$$

$$\text{with} \quad H(\mathrm{j}\omega) = h_0 \frac{\omega_0 \tau^2}{(1+\mathrm{j}\omega\tau)^2 + \tau^2\omega_0^2} \exp(-\mathrm{j}\omega t_0). \tag{10}$$

For convenience, we choose the time of arrival $t_0 = 0$. Thus we obtain

$$|F_x(\mathrm{j}\omega)|^2 = \frac{h_0^2 L^2 \omega_0^2 m_x^2}{4} \frac{\omega^4}{\left(\omega^2 - \omega_5^2\right)\left(\omega^2 - \omega_6^2\right)} \tag{11}$$

$$\text{with} \quad \omega_5 = -\omega_0 + \mathrm{j}/\tau \qquad \omega_6 = -\omega_5^* \tag{12}$$

that describes a Lorentzian centred and peaked at $f = f_0$ (see figure 1). Its peak value is

$$|F_x(\mathrm{j}\omega_0)| \approx m_x L h_0 \omega_0^2 \tau \big/ 4 \qquad \text{for} \quad \omega_0\tau \gg 1. \tag{13}$$

As τ increases, $h(t)$ tends to a periodic signal and hence $|F_x(\mathrm{j}\omega)|$ becomes narrower and narrower. The larger the damping time, the longer is the duration of $h(t)$ and the larger is the energy imparted to the detector when in resonance. This is indicated by the linear dependence of $|F_x(\mathrm{j}\omega_0)|$ on τ (hence on the number of cycles).

We recall that the impulse response of the bar–transducer system is a sum of two damped harmonic oscillations with decay times $\tau'_{\pm}$ ($\sim$ a few hundred seconds) [4]. As the signal itself that we are considering has a damped sinusoidal profile, we expect the signal poles ($\omega_{5,6}$) to have a similar appearance to the system poles, namely $\omega_{1,2}$ (plus resonance) and $\omega_{3,4}$ (minus resonance), see equations (6), (7), (12).

In the limit $\tau \to 0$, that is when $h(t)$ is delta-like (impulse limit) we have in particular $\omega_+\tau \ll 1$. This implies that the signal $|H(\mathrm{j}\omega)|^2$ has a flat spectrum in the BW (at least up to f_+) and therefore $|F_x(\mathrm{j}\omega)| \sim m_x L h_0 \omega_0 \omega^2 \tau^2/2$.[6]

In the general case, from equations (4)–(12), we get

$$u(t) = \frac{-h_0 L \omega_0 \tau^2}{4\pi} \int_{-\infty}^{\infty} \frac{\omega^4 \exp(\mathrm{j}\omega t)}{[(1+\mathrm{j}\omega\tau)^2 + \tau^2\omega_0^2] \prod_{i=1}^{4} (\omega - \omega_i)} \,\mathrm{d}\omega, \tag{14}$$

where the integrand has six poles, ω_k, $k = 1, \ldots, 6$, as given in equations (6), (7), (12).

We perform the integration in equation (14) using the residue theorem [8]. Following this, the evaluation of the right-hand side of equation (14) amounts to summing the residues of the integral within the region of convergence (positive half complex plane), i.e.

$$u(t) = \frac{-h_0 L \omega_0 \tau^2}{4\pi} 2\pi\,\mathrm{j} \sum_k R_k. \tag{15}$$

The residue of the integral at the kth pole is

$$\mathrm{R}_k = \frac{-\omega_k^4 \exp(\mathrm{j}\omega_k t)}{\tau^2 \Pi_{i,i\neq k}(\omega_i - \omega_k)}, \qquad i = 1, \ldots, 6. \tag{16}$$

The result of the integration can be written as a sum of three contributions, corresponding to the poles, respectively, of the plus mode, the minus mode and the 'signal mode', i.e.

$$u(t) = u_+(t) + u_-(t) + u_s(t). \tag{17}$$

3.1. Response associated with the modes

The term, $u_\pm(t)$, associated with the mechanical resonances can be obtained from equations (6), (15), (16) as

$$\begin{aligned} u_\pm(t) &= \pm \frac{h_0 L \omega_0 \tau^2}{2} \frac{\omega_\pm^3 \exp(-\beta_\pm t)}{\left(\omega_+^2 - \omega_-^2\right)|T_\pm|} \sin(\omega_\pm t - \arg(T_\pm)) \\ &\equiv \pm E_\pm(t) \sin(\Phi_\pm(t)), \end{aligned} \tag{18}$$

where $T_\pm = -\tau^2[(\omega_{1/3} - \omega_5)(\omega_{1/3} - \omega_6)]$. The notation $1/3$ implies that for T_+ we use ω_1; for T_-, ω_3.

Assuming $\beta_\pm \ll 1$, we get

$$T_\pm \sim \left[1 - \tau^2\left(\omega_\pm^2 - \omega_0^2\right)\right] + 2\mathrm{j}\omega_\pm\tau. \tag{19}$$

We note that the external force f_x affects the phase as well as the amplitude of the modes via $T_\pm$ as shown in equation (18). When the signal frequency gets close to the resonances, i.e. $f_0 \to f_\pm$, $|T_\pm|$ decreases and $u_\pm(t)$ oscillates with increasing amplitude because the mode extracts more energy from the signal since the mode is in resonance with it. This can be also inferred from equation (14).

In the impulse limit, $\tau \to 0$, in particular $\tau \ll 1/\omega_+$, we have $T_\pm \to 1$ and

$$u_\pm(t) \sim \pm \frac{h_0 L \omega_0 \tau^2}{2} \frac{\omega_\pm^3 \exp(-\beta_\pm t)}{\left(\omega_+^2 - \omega_-^2\right)} \sin(\omega_\pm t). \tag{20}$$

We note that in this limit, as expected, equation (20) agrees with the impulse response of the bar–transducer system given by equation (1.21) of [4].

[6] This expression differs from f_0 as given in footnote (3) of [4] because here we assume $h(t)$ to be delta-like as opposed to the assumption of $f_x(t)$ to be delta-like.

3.2. Response associated to the signal mode

The term $u_s(t)$ associated with the signal can be obtained from equations (12), (15), (16) as

$$\begin{aligned} u_s(t) &= \frac{-h_0 L}{2} \frac{\left(1+\omega_0^2\tau^2\right)^4 \exp(-t/\tau)}{|T_s|} \sin(\omega_0 t - \arg(T_s)), \\ &\equiv E_s(t)\sin(\Phi_s(t)), \end{aligned} \tag{21}$$

where $T_s = \tau^8\omega_5^4\Pi_{i=1,2,3,4}(\omega_5 - \omega_i)^*$.

Using $\beta_\pm \ll 1$, one can simplify $|T_s|$ as

$$|T_s| \sim \left(1+\omega_0^2\tau^2\right)^2 |T_+||T_-|. \tag{22}$$

Thus, the system parameters alter the phase as well as the amplitude of the signal mode via T_s as shown in equations (21), (22). In the impulse limit, $T_s \to 1$ and $E_s(t) \to 0$. Thus, $u(t) = u_+(t) + u_-(t)$ as expected.

3.3. Maximum of $u(t)$ as a function of parameters

Before we proceed into the analytical details of the behaviour of the displacement as a function of the signal and system parameters, we show the result of a simulation where we have studied the maximum of the system response $u(t)$ as a function of the signal parameters, since this quantity determines the signal-to-noise ratio (SNR). Throughout this study, we use the values of the system parameters pertaining to the Explorer detector in the year 2005 (see section 4 for details).

In figure 2(*a*), we plot the maximum M_u of the displacement $u(t)$ as a function of f_0 for fixed values of τ. It can be seen that, for a given τ, as f_0 approaches the resonances ($f_- = 904.7$ Hz, $f_+ = 927.452$ Hz), the value of the maximum increases sharply as energy is transferred to the $\pm$ modes more efficiently due to the resonant condition. For small τ (less than $\approx$20 ms), the behaviour is almost flat, as expected, while, as τ increases the difference between the resonant situation (signal frequency near the resonances) and the non-resonant one becomes more and more prominent, e.g., for $\tau = 0.2$ s, the difference between M_u at $f_0 = f_\pm$ and $f_0 = 915$ Hz (worst case between the resonances) is a factor of $\approx$8, which will be translated in SNR.

In figure 2(*b*) we plot the maximum M_u as a function of τ for fixed values of the signal frequency f_0. We note that for f_0 close to the resonances, this maximum increases quite rapidly with τ, in contrast to when f_0 is away from the resonances. In fact, in the latter case, increasing τ does not increase the amplitude substantially: when the signal frequency is away from resonance, the energy transferred in the resonant modes is almost constant after the initial increase.

3.4. Envelope and phase of the response $u(t)$

As discussed earlier, the system response $u(t)$ is amplitude and phase modulated. In fact, using equations (18), (21), we can write $u(t)$ as

$$u(t) = E(t)\sin[\Phi(t)], \tag{23}$$

where the envelope and the phase are

$$E(t) = A^2 + E_s^2 + 2E_s A\cos(\Delta\Phi_2), \tag{24}$$

$$\Phi(t) = \Phi_s(t) + \tan^{-1}\left[\frac{A\sin(\Delta\Phi_2)}{A\cos(\Delta\Phi_2) + E_s}\right], \tag{25}$$

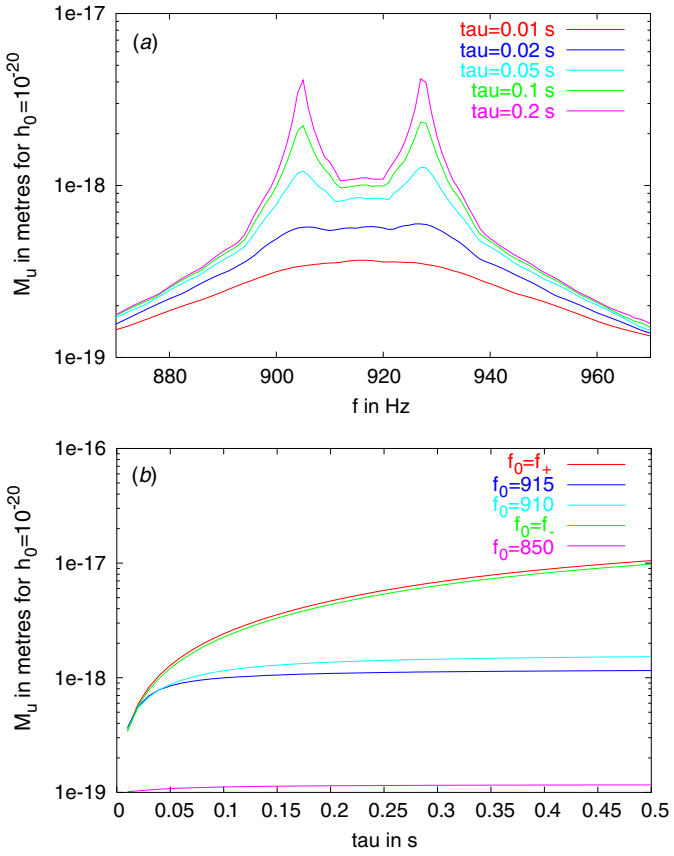

Figure 2. Maximum displacement M_u versus f_0 for various τ (a) and versus τ for various f_0 (b). The amplitude of the input signal is fixed to $h_0 = 10^{-20}$. See the text for explanation.

with

$$\Delta\Phi_1 = \Phi_-(t) - \Phi_+(t), \tag{26}$$

$$\Delta\Phi_2 = \Phi_-(t) - \Phi_s(t) - \tan^{-1}\left[\frac{E_- \sin(\Delta\Phi_1)}{E_+ - E_- \cos(\Delta\Phi_1)}\right], \tag{27}$$

$$A^2 = E_+^2 + E_-^2 - 2E_+E_- \cos(\Delta\Phi_1). \tag{28}$$

- Envelope of $u(t)$:
  The modulation of the envelope $E(t)$ depends on the frequency of each term in equation (24). The term A depends only on the beating of the two resonance frequencies of the system, whereas the term $\cos(\Delta\Phi_2)$ depends on both the beating of two resonant frequencies as well as the beating of the signal frequency with the system resonances, see equation (27). This makes the modulation more complex to understand as compared to that in the impulse limit where $E(t) = A(t)$. We demonstrate this complexity in the simple case shown in figure 3, where we assume $f_- = 900$ Hz, $f_+ = 950$ Hz and the signal frequency $f_0 = 910$ Hz with $\tau = 0.5$ s. Here, $f_+ - f_- = 5(f_0 - f_-)$. Thus,

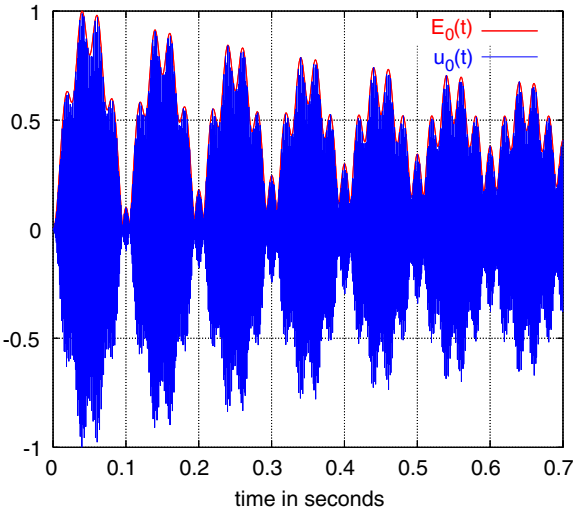

Figure 3. Normalized displacement $u_0(t)$ and normalized envelope $E_0(t)$ for a toy case with $f_+ = 950$ Hz, $f_- = 900$ Hz, $f_0 = 910$ Hz. See the text for explanations.

$A\cos(\Delta\Phi_2)$ oscillates with $(f_0 - f_-) = 10$ Hz. Since A^2 oscillates with $(f_+ - f_-) = 50$ Hz, the envelope modulates with the frequency $(950 - 900)/5 = 10$ Hz, as it appears in figure 3. The five bumps with period of 0.1 s correspond to phase modulation of the envelope with the frequency of 50 Hz. The phase of the envelope oscillates with frequency $910 - 900 = 10$ Hz.

- Phase of $u(t)$:

  As shown in equation (24), the signal introduces additional phase $\Phi_s(t)$. Further, the coupling of the signal to the system introduces an extra phase due to E_s. As a result, the phase modulation of the displacement depends on both system as well as signal parameters.

4. Study of the system response for specific cases

In what follows we shall illustrate the above results using the parameters of Explorer, with $M_{\rm bar} = 2230$ kg and $L_{\rm bar} = 3$ m. Similar results can be obtained for Nautilus or any other two mode resonant bar. We assume the Feb. 2005 Explorer configuration, with resonance frequencies $f_- = 904.7$ Hz, $f_+ = 927.452$ Hz and decay times $\tau'_+ = 1/\beta_+ = 521.24$ s and $\tau'_- = 1/\beta_- = 961.26$ s.

In figure 4 we plot the noise spectral density of Explorer, with BW of ~ 20 Hz at the level of $\sqrt{S_n} \sim 10^{-20}\,{\rm Hz}^{-1/2}$. We define the sensitive frequency band of the detector as FB $\sim \{900, 932\}$ Hz. This choice is done noticing that at 900 Hz and at 932 Hz the noise spectrum has roughly the same value, i.e. $\sqrt{S_n} \sim 10^{-20}\,{\rm Hz}^{-1/2}$, as the worst value between the resonances (at the frequency $f = (f_+ + f_-)/2 \sim 915$ Hz).

Such a choice is made in order to study the detector response in two distinct cases; namely, (1) f_0 within the FB, the sensitive band of the detector, (2) f_0 outside the FB, that is away from the sensitive band, which will help us to illustrate various features of the response.

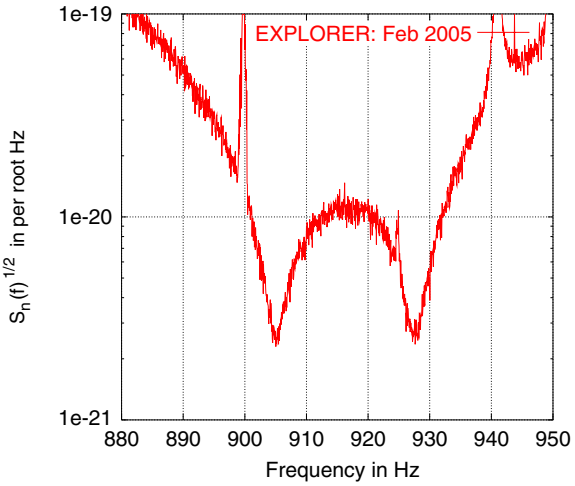

Figure 4. Explorer (Feb. 2005): two sided amplitude spectral density $\sqrt{S_n}$ in units of strain per root Hz.

4.1. Case 1: f_0 within the FB

Here we study the detector response when $f_0 \in$ FB and $\tau \in \{0.01, 0.2\}$ s. To begin with, we consider two special cases: (a) most sensitive case for $f_0 = f_\pm$; (b) worst sensitive case, for $f_0 \sim 915$ Hz.

4.1.1. Case 1(A) $f_0 = f_\pm$. Let $f_0 = f_+$ and $\tau \in \{0.01, 0.2\}$ s. Figure 5 shows the normalized displacement $u_0(t)$, as a function of time, for increasing values of τ. The response for small values of τ ($\leqslant 10$ ms, with these parameters) is, as expected, similar to the impulse response. In fact, in the frequency domain, this corresponds to a flat behaviour of the Lorentzian $|F_x(\mathrm{j}\omega)|$. A flat Lorentzian over the considered FB leads to a response which does not depend on the signal frequency but just on the beating of the two resonances.

As τ increases, the incoming signal tends to a periodic signal with frequency f_+ and duration $\sim\tau$ and hence the displacement $u_0(t)$ gradually changes from the impulse response to the forced sinusoidal response in the resonance condition. In particular, the position of the maximum t_m depends on τ. We recall here that, as was shown in figure 2, the value of the maximum increases with τ. Here, we obtain this expression analytically. Using equations (19), (22) and $\omega_0 = \omega_+$, we get

$$|T_+| \sim 2\omega_+\tau, \qquad |T_-| \sim \tau^2\left(\omega_-^2 - \omega_+^2\right), \tag{29}$$

$$|T_s| \sim 2\omega_+^5\tau^7\left(\omega_-^2 - \omega_+^2\right), \tag{30}$$

and then

$$E_+(t_m) \sim \frac{h_0 L\omega_+^3\tau}{4\left(\omega_+^2 - \omega_-^2\right)}, \qquad E_-(t_m) \sim \frac{h_0 L\omega_+\omega_-^3}{2\left(\omega_+^2 - \omega_-^2\right)^2},$$

$$E_s(t_m) \sim \frac{-h_0 L\omega_+^3\tau}{4\left(\omega_+^2 - \omega_-^2\right)} \exp(-t_m/\tau).$$

In the above the behaviour of $E_+(t_m)$ is different from that of $E_-(t_m)$ because here we are considering the case of $\omega_0 = \omega_+$. We also note, from equations (18), (21), that most of the

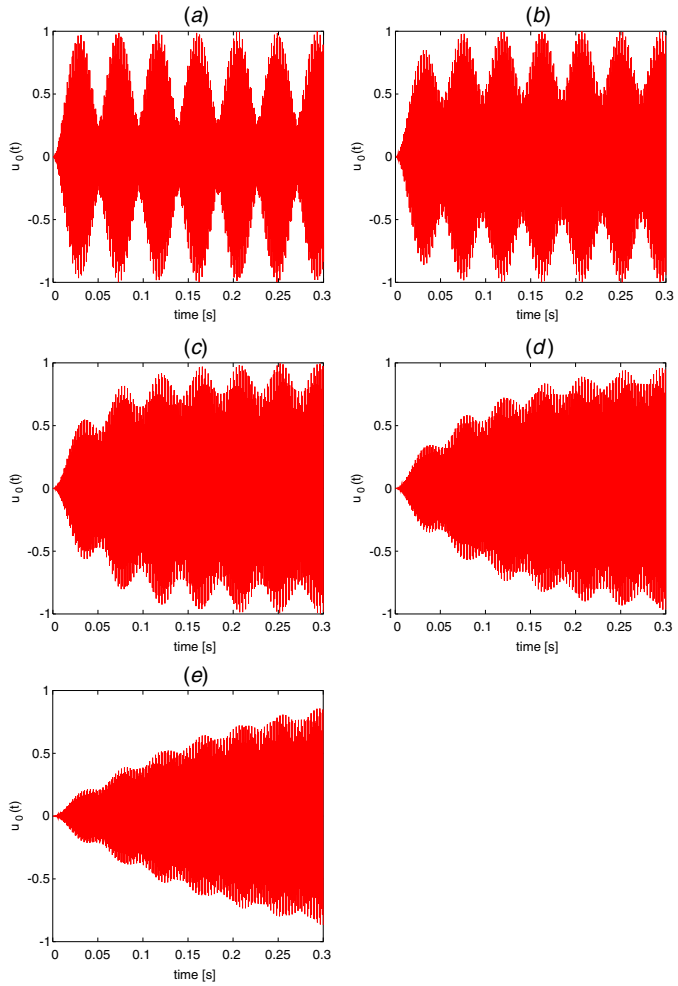

Figure 5. Case 1(A). Normalized displacement $u_0(t)$ for $f_0 = f_+ = 927.4$ Hz and (*a*) $\tau =$ 10 ms, (*b*) 20 ms, (*c*) 50 ms, (*d*) 100 ms, (*e*) 200 ms. For small τ the displacement is, as expected, similar to the impulse response. As τ increases it tends gradually to be different from the impulse response, and the position t_m of the maximum depends on τ.

signal energy gets transferred to the system in the timescale of $t \simeq 2\tau_m$, followed by the decay of the modes (ringing of the bar) which in its turn depends on the $\tau'_{\pm}$. We further note that in this case the phase of the envelope oscillates with the beat frequency $(f_+ - f_-)$.

It is easy to understand that the case $f_0 = f_-$ leads to results similar to the above, because the behaviour of the detector at the two resonances is in general the same. In addition, in this particular situation, the two resonances also have roughly the same parameters (width, sensitivity).

4.1.2. Case 1(B) $f_0 = 915\,Hz$. Let $f_0 = 915$ Hz ($(f_+ + f_-)/2$ in this case) and $\tau \in \{0.01, 0.2\}$ s. Figure 6 shows the normalized displacement $u_0(t)$, as a function of time, for various values of τ. Now the signal frequency is not one of the resonances and thus we expect different behaviour of the response, compared to the previous case.

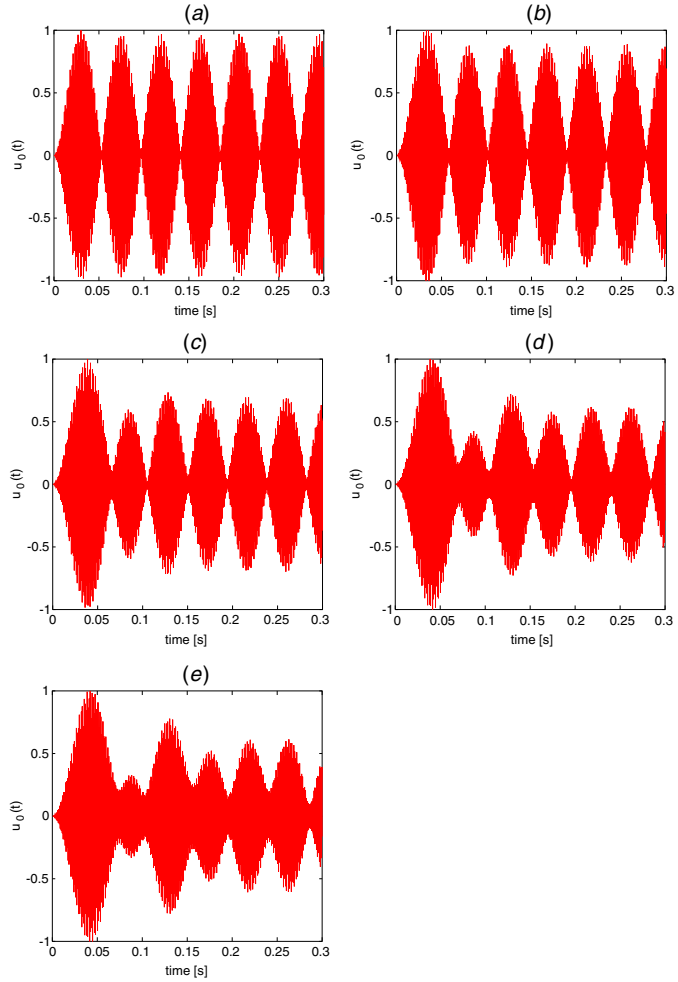

Figure 6. Case 1(B). Normalized displacement $u_0(t)$ for $f_0 = 915$ Hz and (*a*) $\tau = 10$ ms, (*b*) 20 ms, (*c*) 50 ms, (*d*) 100 ms, (*e*) 200 ms.

First, we note that, for small values of τ, the response is still similar to the impulse response, as expected from the earlier discussion.

We expect differences as τ increases. In fact, as τ increases, both the resonances fall on a tail of the input Lorentzian and equal energy is imparted to both the resonances. This makes the time t_m of the maximum displacement constant with respect to τ: a feature quite different from the previous case. Further, we note that the energy given to the system is much smaller compared to when $f_0 \sim f_\pm$, as shown by the behaviour of M_u in figure 2. Hence, in this situation, for large values of τ, as shown below, the maximum does not depend on τ (the figures are normalized, so this cannot be seen from them). In fact, if we let $\tau > \max\{10/|\omega_+ - \omega_0|, 10/|\omega_- - \omega_0|\}$, then we get, from equation (19),

$$|T_+| \sim \tau^2|\omega_+^2 - \omega_0^2|, \qquad |T_-| \sim \tau^2\left|\omega_-^2 - \omega_0^2\right| \tag{31}$$

$$|T_s| \sim \omega_0^4\tau^4|T_+||T_-|, \tag{32}$$

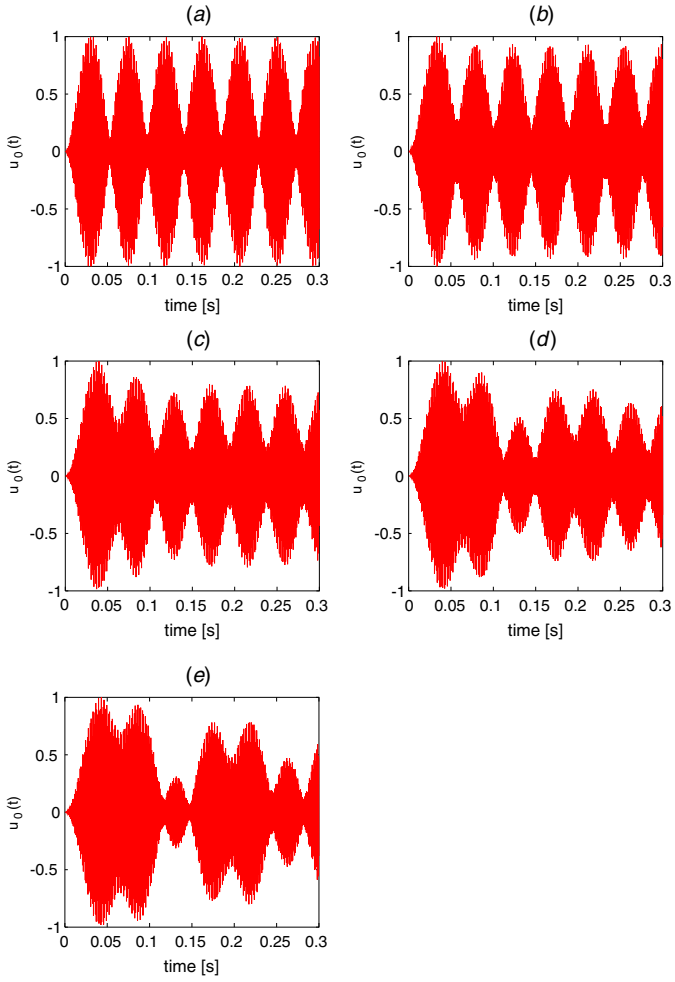

Figure 7. Case 1(C). Normalized displacement $u_0(t)$ for $f_0 = 920$ Hz and (*a*) $\tau = 10$ ms, (*b*) 20 ms, (*c*) 50 ms, (*d*) 100 ms, (*e*) 200 ms. This figure is indicative when compared with those of cases 1(A) and (B): the comparison of the three cases A, B, C, for a fixed τ, shows how $u_0(t)$ gets modulated for different frequencies.

from which we estimate

$$M_u \sim \frac{h_0 L \omega_0}{2} \left[\frac{\omega_+^3(\omega_0^2 - \omega_-^2) + \omega_-^3(\omega_+^2 - \omega_0^2) + \omega_0^3(\omega_+^2 - \omega_-^2)}{(\omega_+^2 - \omega_-^2)(\omega_+^2 - \omega_0^2)(\omega_0^2 - \omega_-^2)} \right]. \tag{33}$$

Thus, for a given signal frequency, the quantity $\max\{10/|\omega_+ - \omega_0|, 10/|\omega_- - \omega_0|\}$ gives that τ after which M_u becomes constant (see figure 2(*b*)). For example, if $f_0 \sim 915$ Hz, we get, with the above condition on the maximum, a value of $\tau \sim 130$ ms, which agrees with the value plotted in figure 2(*b*).

In general, for other excitation frequencies within the FB range, the modulation of the response will depend upon the relative beating of the frequencies f_+, f_-, f_0. As an example, we plot $u_0(t)$ for $f_0 = 920$ Hz for different τ in figure 7 (case 1(C). Further, for a fixed τ, how

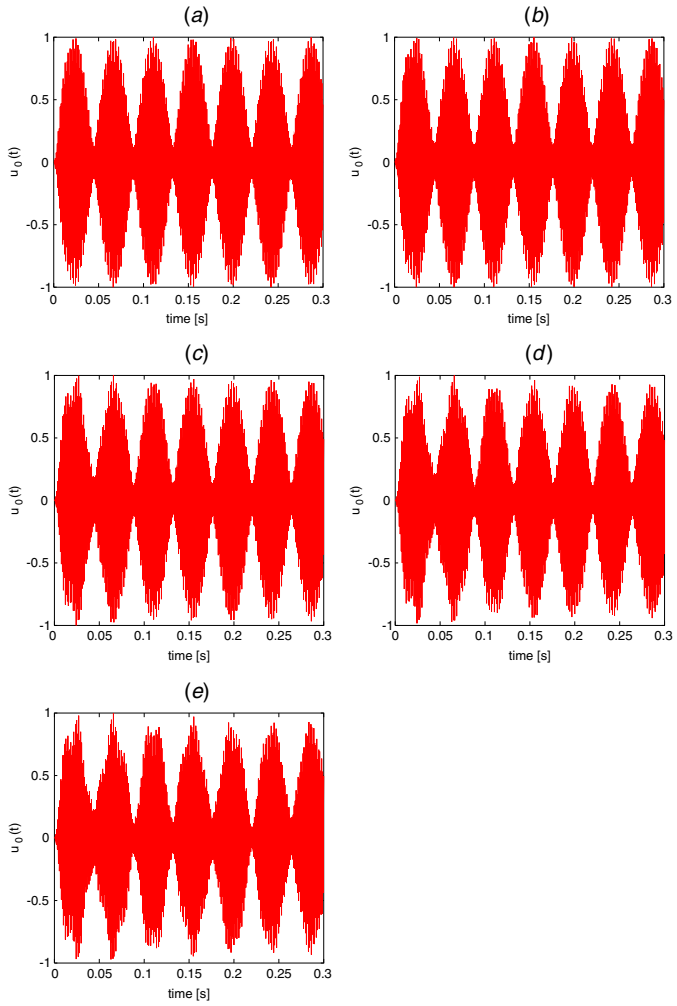

Figure 8. Case 2. Normalized displacement $u_0(t)$ for $f_0 = 850$ Hz and (*a*) $\tau = 10$ ms, (*b*) 20 ms, (*c*) 50 ms, (*d*) 100 ms, (*e*) 200 ms. In this situation, for all the considered τ, the response is similar to the impulse response, and the energy which the signal releases to the system is always very small. See the text for comments.

$u_0(t)$ gets modulated for different frequencies can be seen by comparing the corresponding case in figures 5, 7, 6.

4.2. Case (2): f_0 outside the FB

We consider here an excitation frequency f_0 far from the FB with $\tau \in \{0.01, 0.2\}$ s. As shown in figure 8, the system response is similar to that of an impulse-like signal both for small and large values of τ. In fact, as τ increases, the FB range still falls on the tail of the Lorentzian, with roughly the same value of $|F_x(\mathrm{j}\omega)|$ at the two resonances, such that the response stays close to the impulse response. Further, as discussed earlier, for a given excitation frequency $\max\{10/|\omega_+ - \omega_0|, 10/|\omega_- - \omega_0|\}$ decides the flatness of M_u. For this case, since f_0 is far from $f_\pm$, $|\omega_\pm - \omega_0|$ is larger and hence $\max\{10/|\omega_+ - \omega_0|, 10/|\omega_- - \omega_0|\}$ is smaller. This

shows that as f_0 goes away from the FB, the input signal mimics an impulse-like signal. Note that the energy released to the modes is very small and so will the SNR be.

5. Optimal detection: matched filtering

For a signal of known shape in a Gaussian stationary noise, matched filtering is an optimal detection strategy. Usually, we consider the filtering of the signal at the output of the electronic chain. Below, we discuss the signal, the noise spectrum and the matched filtering approach.

5.1. Signal

The displacement of the transducer $u(t)$, in units of length, is processed first by the transducer, which provides the voltage $v_t(t) = \alpha u(t)$, and then by the following electronic chain, which has an amplification factor of A. The electrical signal (in volts) at the output of the electronic chain is therefore

$$v(t) = (\alpha A)u(t) \qquad \text{in units of volts} \tag{34}$$

$$\equiv M_v u_0(t) \tag{35}$$

where $u_0(t)$ is the normalized displacement and $M_v \equiv (\alpha A)M_u$.

5.2. Noise

The noise $n(t)$ at the output of the electronic chain is assumed to be coloured Gaussian. The expected noise power spectral density $S_t(\omega)$ consists in fact of [4]:

- a narrow-band noise contribution S_{nb} from the thermal noise of the two mechanical oscillators and the back-action contribution from the transducer, given by

$$S_{nb}(\omega) = \alpha^2 S_{fx}|W_{ux}(\mathrm{j}\omega)|^2 + \alpha^2 S_{fy}|W_{uy}(\mathrm{j}\omega)|^2 \tag{36}$$

  where S_{fx} and S_{fy} are the total noise force spectra on the two oscillators due to the Nyquist (thermal) and the back-action force; W_{ux} and W_{uy} are the system transfer functions from a force applied respectively to the bar and the transducer, and the output displacement;
- a broad-band noise contribution S_e from the electronics, which is assumed to have a flat spectrum in the bandwidth of the detector.

Thus, the expected noise power spectrum related to the transducer output is given by

$$S_t(\omega) = S_e + \alpha^2 S_{fx}|W_{ux}(\mathrm{j}\omega)|^2 + \alpha^2 S_{fy}|W_{uy}(\mathrm{j}\omega)|^2. \tag{37}$$

Besides, there might be other spurious noise sources which can give rise to non-stationarity in the data. However, here we assume that the data under process are stationary.

5.3. Matched filter

In GW detection the signal detection problem involves computing a statistic, a functional of the observed data $z(t)$ which when passed through a threshold allows one to opt for one of the two hypotheses:

$$H1 : z(t) = n(t) + v(t) \qquad \text{signal present}$$

$$= n(t) + M_v u_0(t) \tag{38}$$

$$H0 : z(t) = n(t) \qquad \text{signal absent.} \tag{39}$$

For a signal with known shape in Gaussian and stationary noise the matched filter is an optimal filter. The transfer function of the filter matched to $v(t)$ in the presence of noise with spectrum $S_t(\omega)$ is

$$Q(\mathrm{j}\omega) = N_u \frac{U_0^*(\mathrm{j}\omega)}{S_t(\omega)}, \tag{40}$$

where N_u is a normalization factor in units of volts^2 such that

$$\frac{1}{2\pi}\int_{-\infty}^{\infty} \frac{N_u |U_0^*(\mathrm{j}\omega)|^2}{S_t(\omega)}\,\mathrm{d}\omega = 1, \tag{41}$$

and $U_0(\mathrm{j}\omega)$ is the FT of $u_0(t)$. The matched filter output is given by

$$o(t) = \langle z, q\rangle \tag{42}$$

$$\equiv \frac{1}{2\pi}\int_{-\infty}^{\infty} Z(\mathrm{j}\omega)\,Q(\mathrm{j}\omega)\exp(\mathrm{j}\omega t)\,\mathrm{d}\omega. \tag{43}$$

In the absence of noise, $z(t) = v(t)$ and the output is

$$o(t) = \langle v, q\rangle, \tag{44}$$

$$= \frac{M_v}{2\pi}\int_{-\infty}^{\infty} \frac{N_u |U_0(\mathrm{j}\omega)|^2}{S_t(\omega)}\exp(\mathrm{j}\omega t)\,\mathrm{d}\omega, \tag{45}$$

$$= M_v \frac{N_u g(t)}{M_u^2}. \tag{46}$$

Using the above normalization we get $\max(o(t)) = M_v$. The corresponding time instant is the estimated arrival time of the GW (t_0 in equation (1)). The amplitude of the input signal can be estimated from the maximum of the filtered data M_v. The time-dependent part of $o(t)$, which we call $g(t)$, is in units of V^2 m^{-2} and is given by

$$g(t) = \frac{1}{2\pi}\int_{-\infty}^{\infty} \frac{|U(\mathrm{j}\omega)|^2}{S_t(\omega)}\exp(\mathrm{j}\omega t)\,\mathrm{d}\omega. \tag{47}$$

We note that the FT of $g(t)$, $G(\mathrm{j}\omega)$, has six poles, namely $p_i, i = 1,\ldots,6$, with $p_5 = \omega_5$ and $p_6 = \omega_6$. The function $G(\mathrm{j}\omega)$ can be expressed in terms of the output $G^\delta(\mathrm{j}\omega)$ of a filter matched to a delta-force input as $G(\mathrm{j}\omega) \equiv G^\delta(\mathrm{j}\omega)|F_x(\mathrm{j}\omega)|^2$. Thus from equation (47) we have

$$g(t) = \frac{1}{2\pi}\int_{-\infty}^{\infty} G^\delta(\mathrm{j}\omega)|F_x(\mathrm{j}\omega)|^2\exp(\mathrm{j}\omega t)\,\mathrm{d}\omega \tag{48}$$

where

$$G^\delta(\mathrm{j}\omega) = \frac{\omega^4}{S_n m_x^2\left(\omega^2 - p_1^2\right)\left(\omega^2 - p_2^2\right)\left(\omega^2 - p_3^2\right)\left(\omega^2 - p_4^2\right)}, \tag{49}$$

with poles[7]

$$p_1 = -\omega_+ + \mathrm{j}/\tau_+ \qquad p_2 = -p_1^*, \tag{50}$$

$$p_3 = -\omega_- + \mathrm{j}/\tau_- \qquad p_4 = -p_3^*. \tag{51}$$

Here $\tau_+ = 1/|b'|$, $\tau_- = 1/|d'|$, where $b', d' < 0$ and $\tau_\pm$ represent the decay times of the filter impulse response at the two modes. Their values are always much smaller than the decay

[7] The poles of [4] ω_i (as defined in [4]) are related to p_i by $p_1 = -\omega_1$, $p_2 = \omega_2$, $p_3 = -\omega_3$ and $p_4 = \omega_4$.

times $\tau'_{+,-}$ of the bar–transducer system, as they scale with the (square root of the) ratio of the broad-band noise to the narrow-band noise, generally of the order of 10^{-3}.

We compute $g(t)$ from $G(\mathrm{j}\omega)$ by applying the residue theorem as

$$g(t) = \frac{h_0^2 L^2 \omega^2}{4S_n} \mathrm{j} \sum_k \rho_k, \tag{52}$$

where the kth residue is given by

$$\rho_k = \frac{p_k^7 \exp(\mathrm{i} p_k t)}{2\Pi_{i,k\neq i}\left(p_k^2 - p_i^2\right)}. \tag{53}$$

Substituting equation (53) into equation (52) and simplifying we get

$$g(t) = \frac{-h_0^2 L^2 \omega_0^2}{16 S_n} \Re\left[\frac{\tau_+ \exp(-t/\tau_+)}{\omega_+} \frac{p_1^7 \exp(-\mathrm{j}\omega_+ t)}{\Pi_{k,k\neq 1,2}\left(p_1^2 - p_k^2\right)} + \frac{\tau_- \exp(-t/\tau_-)}{\omega_-} \frac{p_3^7 \exp(-\mathrm{j}\omega_- t)}{\Pi_{k,k\neq 3,4}\left(p_3^2 - p_k^2\right)} + \frac{\tau \exp(-t/\tau)}{\omega_0} \frac{p_5^7 \exp(-\mathrm{j}\omega_0 t)}{\Pi_{k,k\neq 6,8}\left(p_5^2 - p_k^2\right)}\right]. \tag{54}$$

In figure 9, we plot the normalized output of the matched filter for $f_0 = f_-$ (for the second resonance we expect similar results) and $\tau = 0.01, 0.2, 1$ s. We show in 9(a) that, when $\tau < \tau_\pm$, the decay time of the matched filtered output is dominated by $\tau_\pm (\sim 140$ ms). As τ increases and becomes larger than $\tau_\pm$ (see figures 9(b), (c)), the decay time of the filtered output waveform increases due to the contribution of the signal term. As a result, the absolute maximum would decay slowly (closeby time bins would give values similar to the maximum value). In a real situation, with noise, this would increase the arrival timing error, in spite of the increase of SNR with τ, as indicated in figures 10(a), (b).

5.4. Matched filter SNR

The (amplitude) signal-to-noise ratio (SNR) of the matched filter is given by the ratio between the maximum of the filtered output signal and the root mean square value of the output noise:

$$\mathrm{SNR}^2 = \frac{\max(o(t))^2}{\mathrm{Var}(\langle n, q\rangle)}. \tag{55}$$

The maximum of the filtered output $o(t)$ is related to $g(t = 0)$ where

$$g(0) = \frac{-h_0^2 L^2 \omega_0^2}{16 S_n} \Re\left[\frac{\tau_+ p_1^7}{\omega_+ \Pi_{k,k\neq 1,2}\left(p_1^2 - p_k^2\right)} + \frac{\tau_- p_3^7}{\omega_- \Pi_{k,k\neq 3,4}\left(p_3^2 - p_k^2\right)} + \frac{\tau p_5^7}{\omega_0 \Pi_{k,k\neq 6,8}\left(p_5^2 - p_k^2\right)}\right]. \tag{56}$$

Appendix A provides an alternative/independent time domain calculation of $g(0)$.

The maximum of the signal is $\max(o(t)) = M_v$ and the variance of the filtered noise is N_u, as shown in appendix B. Thus we have

$$\mathrm{SNR}^2 = \frac{M_v^2}{N_u} = (\alpha A)^2 g(0) \tag{57}$$

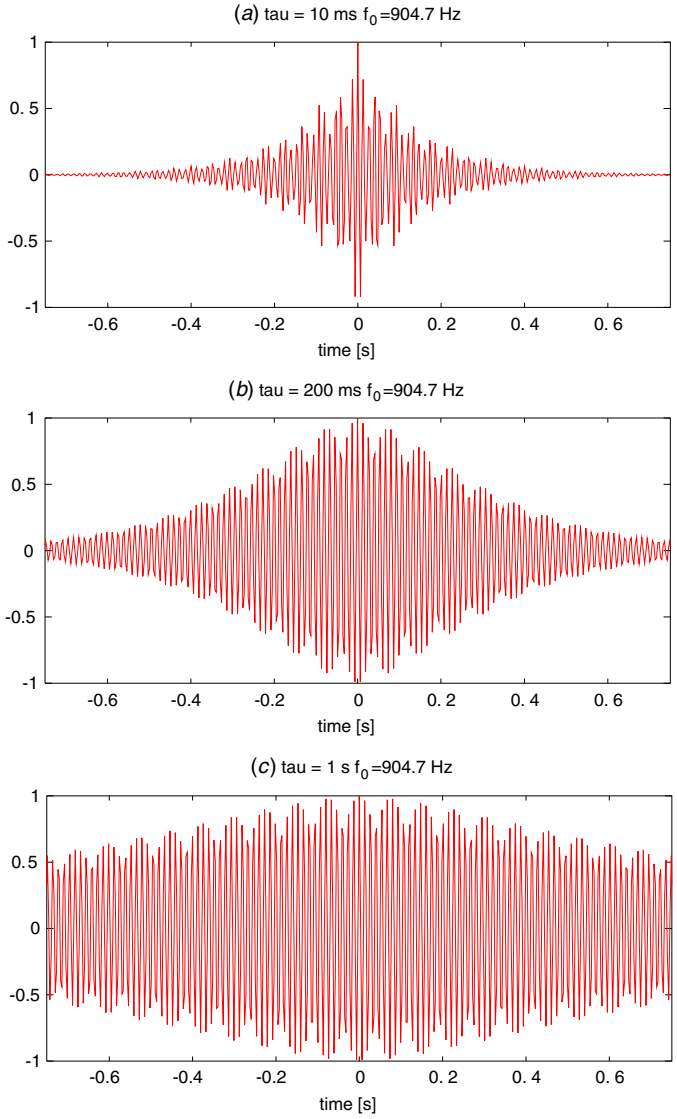

Figure 9. Normalized $g(t)$ for $\tau = 10$ ms (a), 0.2 s (b), 1 s (c) and signal frequency $f_0 = f_-$, with $\tau'_\pm \approx 140$ ms.

which can be written as:

$$\mathrm{SNR}^2 = \frac{M_v^2}{N_u} = \frac{1}{2\pi}\int_{-\infty}^{\infty} \frac{|V(\mathrm{j}\omega)|^2}{S_t(\omega)}\,\mathrm{d}\omega, \tag{58}$$

where $V(\mathrm{j}\omega)$ is the FT of $v(t)$.

The essential features of the filtered response become evident in the SNR plots given in figures 10(a), (b), (c): (1) The SNR increases with τ for any excitation frequency as the signal spends a large number of cycles in the detector band. (2) This increase in SNR is quite large in the resonant condition when $f_0 = f_\pm$. (3) For large τ the uncertainty in the arrival time

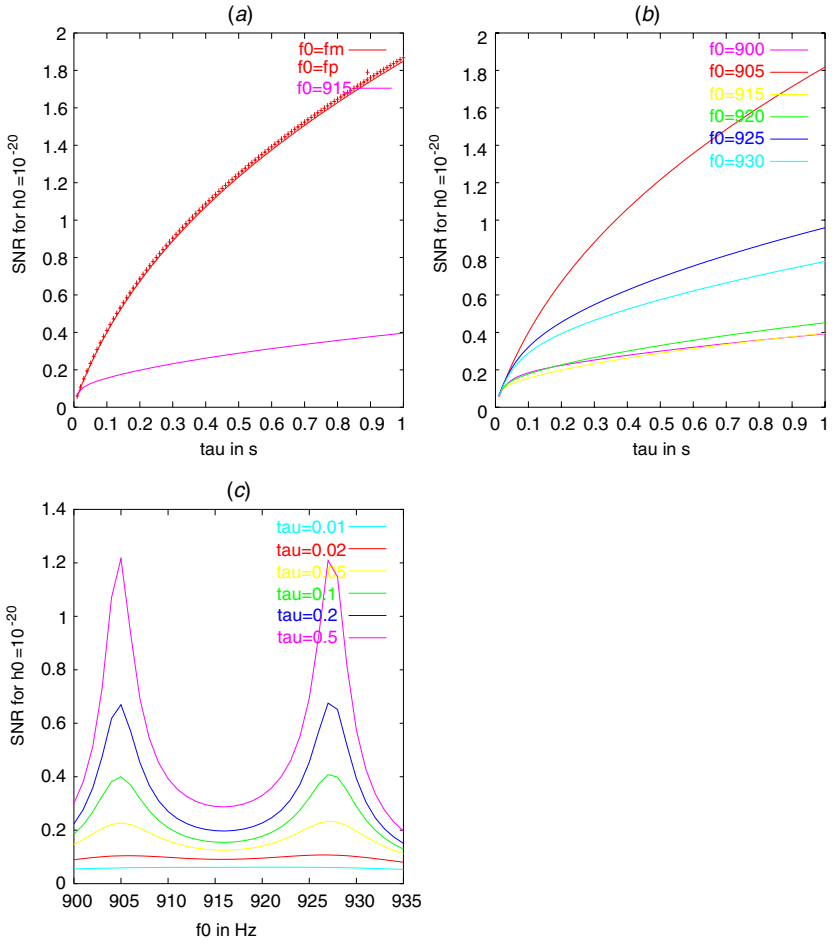

Figure 10. $h_0 = 10^{-20}$: (*a*) SNR versus τ for $f_0 = f_{\pm}$, 915 Hz, (*b*) SNR versus τ for $f_0 \in$ FB, (*c*) SNR versus f_0 for $\tau \in \{0.01, 0.5\}$ s.

due to the noise increases, while at the same time the SNR increases. We plan to perform simulations in the presence of noise, to obtain quantitative information on this point.

6. Conclusion

In this work we studied the response of a resonant GW detector to damped sine-wave signals in detail as well as the characteristics of the signal after a filter matched to these signals. This study was motivated by the results from an earlier study [9], where we computed the SNR loss when a damped sinusoidal signal was processed with a filter matched to a delta function input rather than to a damped sinusoid. We found that for large decay times of the input ($\tau > 50$ ms) and when the signal frequency is in the sensitive frequency band, it is crucial to use a properly matched filter rather than the δ filter. This led us to study the features of the system response to such signals. In this paper, we systematically categorized and studied how the response as well as the SNR depends on the signal parameters.

However, as mentioned earlier, this study represents only a preliminary step in the search for signals which are due to the excitation of stellar quasi-normal modes. In fact here we used a 'toy' model for these signals, which in 'reality' should be characterized by varying frequency and decay time. The next natural step of this study is to obtain the system response for varying frequency and τ input signals and construct a bank of filters or develop a detection strategy for such signals. Further, we wish to extend the detection scheme to a network of detectors comprising both resonant bars and interferometers, which are sensitive over a different, and larger, frequency range, in the view of performing coincidence experiments.

Acknowledgments

The authors would like to thank V Ferrari for bringing into attention the damped sinusoids as one of the sources for resonant detectors. AP gratefully acknowledges INFN for offering the financial support and ICTP (Trieste, Italy) for their support and hospitality.

Appendix A. $g(0)$ obtained from time domain calculation

The output of the matched filter is proportional to

$$g(t) = \int_{-\infty}^{\infty} G^{\delta}(\omega)|F(\omega)|^2 \, \mathrm{e}^{\mathrm{j}\omega t} \, \mathrm{d}\omega = \int_{-\infty}^{\infty} g_{\delta}(t') F_{+-}(t'-t) \, \mathrm{d}t' \tag{A.1}$$

where $g^{\delta}(t)$ (inverse FT of $G^{\delta}(\omega)$) is the matched filter response to a delta input force applied to the bar as given in [4]

$$g^{\delta}(t) = -\frac{1}{4S_n m_x^2}\left[\frac{\exp(b'|t|)[\zeta_1\cos(\omega_+ t) - \zeta_2\sin(\omega_+ t)]}{\omega_+ b'|\left(p_1^2 - p_3^2\right)\left(p_1^2 - p_4^2\right)|^2} + \frac{\exp(d'|t|)[\eta_1\cos(\omega_- t) - \eta_2\sin(\omega_- t)]}{\omega_- d'|\left(p_3^2 - p_1^2\right)\left(p_3^2 - p_2^2\right)|^2}\right] \tag{A.2}$$

$$= g_+^{\delta}(t) + g_-^{\delta}(t) \tag{A.3}$$

where

$$\zeta_1 - \mathrm{j}\zeta_2 = p_1^3\left(p_1^2 - p_3^2\right)^*\left(p_1^2 - p_4^2\right)^* \equiv \sqrt{\zeta_1^2 + \zeta_2^2}\exp(-\mathrm{j}\theta) \tag{A.4}$$

$$\eta_1 - \mathrm{j}\eta_2 = p_3^3\left(p_3^2 - p_1^2\right)^*\left(p_3^2 - p_2^2\right)^* \equiv \sqrt{\eta_1^2 + \eta_2^2}\exp(-\mathrm{j}\xi) \tag{A.5}$$

and $F_{\pm}(t)$ is the inverse FT of $|F(\omega)|^2$ and can be obtained in time domain by convolving the external force $f_x(t)$ with $f_x(-t)$ as given below,

$$F_{\pm}(t) = \int_{-\infty}^{\infty} f_x(t') f_x(t'+t) \, \mathrm{d}t. \tag{A.6}$$

By performing an explicit time domain integration, we get

$$F_{\pm}(t \neq 0) = \frac{h_0^2 l^2 m_x^2}{16}\frac{\omega_0}{\tau^2}\exp\left(-\frac{|t|}{\tau}\right)\left[\omega_0\tau\left(-3 + \tau^2\omega_0^2\right)\cos(\omega_0|t|) + \left(1 - 3\tau^2\omega_0^2\right)\sin(\omega_0|t|)\right]$$

$$\equiv \frac{h_0^2 l^2 m_x^2}{16}\frac{\omega_0}{\tau}\exp\left(-\frac{|t|}{\tau}\right)[A\cos(\omega_0|t|) + B\sin(\omega_0|t|)] \tag{A.7}$$

$$F_{\pm}(0) = \frac{h_0^2 l^2 m_x^2 \omega_0^2}{4}\left[\int_{-\infty}^{+\infty}\delta^2(t)\,\mathrm{d}t - \frac{2}{\tau}\right]. \tag{A.8}$$

Using the definition of delta function and for $\omega_c \to \infty$ [10], we get

$$2\pi\delta(t) = \int_{-\infty}^{\infty} e^{j\omega t}\, d\omega \qquad \int_{-\infty}^{+\infty} \delta^2(t)\, dt = \int_{-\infty}^{+\infty} \frac{\sin^2(\omega_c t/2)}{(\pi t)^2}\, dt = \frac{\omega_c}{2\pi} \equiv \frac{1}{\epsilon}. \tag{A.9}$$

Now, let $\epsilon \to 0$

$$\begin{aligned} g(0) &= \int_{-\infty}^{+\infty} g^{\delta}(t')F_{\pm}(t')\, dt' = \int_{0,\epsilon\to 0}^{\epsilon} g^{\delta}(t')F_{\pm}(t')\, dt' + 2\int_{\epsilon\to 0}^{+\infty} g^{\delta}(t')F_{\pm}(t')\, dt' \\ &= g_0(0) + g_{\pm}(0). \end{aligned} \tag{A.10}$$

We compute the two terms separately as shown below:

$$g_0(0) = \frac{h_0^2 l^2 m_x^2 \omega_0^2}{4} \int_{0,\epsilon\to 0}^{\epsilon} g^{\delta}(t') \left[\frac{1}{\epsilon} - \frac{2}{\tau}\right] dt' = -\frac{h_0^2\omega_0^2 l^2}{8S_n}\left[\frac{\omega_+^2}{b'} + \frac{\omega_-^2}{d'}\right] \tag{A.11}$$

$$g_{\pm}(0) = 2\int_0^{+\infty} g_+^{\delta}(t')F_{\pm}(t')\, dt' + 2\int_0^{+\infty} g_-^{\delta}(t')F_{\pm}(t')\, dt' \equiv g_+(0) + g_-(0). \tag{A.12}$$

Solving the integrals with $\tan(\gamma) = B/A$, we rewrite $g_{\pm}(0)$ as follows:

$$\begin{aligned} g_+(0) &= -\frac{h_0^2 l^2 \omega_0}{32 S_n \omega_+ b'}\left[\frac{(1-b'\tau)\cos[\gamma+\theta] + \tau(\omega_0-\omega_+)\sin[\gamma+\theta]}{(1-b'\tau)^2 + \tau^2(\omega_+-\omega_0)^2}\right. \\ &\quad \left. + \frac{(1-b'\tau)\cos[\gamma-\theta] + \tau(\omega_0+\omega_+)\sin[\gamma-\theta]}{(1-b'\tau)^2 + \tau^2(\omega_++\omega_0)^2}\right] \\ g_-(0) &= -\frac{h_0^2 l^2 \omega_0}{32 S_n \omega_- d'}\left[\frac{(1-d'\tau)\cos[\gamma+\xi] + \tau(\omega_0-\omega_-)\sin[\gamma+\xi]}{(1-d'\tau)^2 + \tau^2(\omega_--\omega_0)^2}\right. \\ &\quad \left. + \frac{(1-d'\tau)\cos[\gamma-\xi] + \tau(\omega_0+\omega_-)\sin[\gamma-\xi]}{(1-d'\tau)^2 + \tau^2(\omega_-+\omega_0)^2}\right]. \end{aligned} \tag{A.13}$$

We express equations (A.11), (A.13) in terms of the poles p_i as follows:

$$g_0(0) = -\frac{h_0^2\omega_0^2 l^2}{2S_n}\Re\left[\frac{p_1^3}{\omega_+(p_1^2-p_3^2)(p_1^2-p_4^2)} + \frac{p_3^3}{\omega_-(p_3^2-p_1^2)(p_3^2-p_2^2)}\right] \tag{A.14}$$

$$g_+(0) = -\frac{h_0^2 l^2 \omega_0 \tau}{32 S_n \omega_+ b'}\Im\left[\frac{p_1^3}{(p_1^2-p_3^2)(p_1^2-p_4^2)}\left(\frac{p_6^3}{p_2^*+p_8^*} - \frac{p_8^3}{p_2^*+p_6^*}\right)\right] \tag{A.15}$$

$$g_-(0) = -\frac{h_0^2 l^2 \omega_0 \tau}{32 S_n \omega_- d'}\Im\left[\frac{p_3^3}{(p_3^2-p_1^2)(p_3^2-p_2^2)}\left(\frac{p_6^3}{p_4^*+p_8^*} - \frac{p_8^3}{p_4^*+p_6^*}\right)\right]. \tag{A.16}$$

Adding equations (A.14), (A.15), (A.16), after some algebraic manipulations, one obtains $g(0)$ as given in equation (56) in section 5.4.

Appendix B. Noise variance of the filtered data

The noise at the input of the matched filter is zero mean, Gaussian process with spectrum $S_t(\omega)$ defined as

$$E(N(j\omega)N^*(j\omega')) \equiv \delta(\omega-\omega')S_t(\omega). \tag{B.1}$$

The variance of the corresponding noise at the output of the filter is

$$\mathrm{Var}(\langle n, q\rangle) = E\{\langle n, q\rangle^2\} - (E\{\langle n, q\rangle\})^2 \tag{B.2}$$

$$\begin{aligned}
&= \frac{1}{(2\pi)^2}\int_{-\infty}^{\infty}\int_{-\infty}^{\infty} E\{N(\mathrm{j}\omega)N^*(\mathrm{j}\omega')\}Q^*(\mathrm{j}\omega)Q(\mathrm{j}\omega')\exp(\mathrm{j}(\omega'-\omega)t)\,\mathrm{d}\omega\,\mathrm{d}\omega' \\
&= \frac{1}{(2\pi)^2}\int_{-\infty}^{\infty}\int_{-\infty}^{\infty} \delta(\omega-\omega')S_t(\omega)Q^*(\mathrm{j}\omega)Q(\mathrm{j}\omega')\exp(\mathrm{j}\omega t)\exp(\mathrm{j}\omega' t)\,\mathrm{d}\omega\,\mathrm{d}\omega' \\
&= \frac{1}{2\pi}\int_{-\infty}^{\infty} S_t(\omega)|Q(\mathrm{j}\omega)|^2\mathrm{d}\omega \\
&= N_u. \qquad \text{(B.3)}
\end{aligned}$$

References

[1] Astone P *et al* 2003 *Phys. Rev. Lett.* **91** 111101 (*Preprint* gr-qc/0307120)
[2] Vinante A *et al* 2006 *Class. Quantum Grav.* **23** S103
[3] De Waard A *et al* 2003 *Class. Quantum Grav.* **20** S143
[4] Astone P, Pallottino G V, Frasca S, Buttiglione C and Pizzella G 1997 *Nuovo Cimento* C **20** 9
[5] Andersson N and Kokkotas K D 2004 *Lectures at the 2nd Aegean Summer School on the Early Universe (Syros, 2003)* (*Preprint* gr-qc/0403087)
[6] Ferrari V, Miniutti G and Pons J A 2003 *Class. Quantum Grav.* **20** S841
[7] Abbott B *et al* 2004 *Phys. Rev.* D **69** 102001 (*Preprint* gr-qc/0312056)
[8] Arfken B and Weber H J 1966 *Mathematical Methods for Physicists* 4th edn (New York: Academic)
[9] D'Antonio S, Pai A and Astone P 2006 *J. Phys. Conf. Ser.* **32** 192
[10] Greiner W and Reinhardt J 1994 *Quantum Electrodynamics* (Berlin: Springer)